Table III
Molecular Weights of the Polymers Eluted below and above the Boundary Temperature (T_b) of the Bimodal SCB Distribution for LLDPE-A to LLDPE-D

	$\bar{M}_w \times 10^{-4}$			
	LLDPE-A	LLDPE-B	LLDPE-C	LLDPE-D
whole polymer	8.3	8.9	9.7	7.4
polymer below T_b[a]	7.0	5.6	8.0	6.6
polymer above T_b	11.1	12.0	12.2	9.1

[a] T_b is the boundary elution temperature between the two peaks of the bimodal SCB distribution curve.

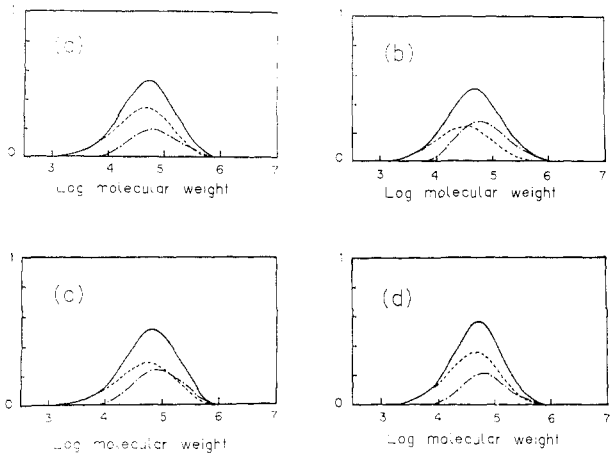

Figure 11. Molecular weight distribution curves of the polymers eluted below and above the boundary temperature (T_b) of the bimodal SCB distribution: (—) whole polymer; (- - -) polymer eluted below T_b; (-·-) polymer eluted above T_b. (a) LLDPE-A; (b) LLDPE-B; (c) LLDPE-C; (d) LLDPE-D.

give the higher molecular weight polymer.

Conclusion

Four LLDPEs manufactured by different processes and one HP-LDPE have been examined by TREF, SEC, ^{13}C NMR, DSC, and FTIR. From these results, the following conclusions were derived:

(1) LLDPEs have an intermolecular bimodal SCB distribution in common.

(2) The bimodal SCB distribution is caused by two kinds of active sites in Ti-based heterogeneous Ziegler catalysts.

(3) One kind of active site has an alternating character of copolymerization, identified by $r_1r_2 = 0.5$–0.6, and the other has a random character, identified by $r_1r_2 = 1.0$.

(4) The sites of $r_1r_2 = 0.5$–0.6 give the higher SCB concentration peak of the bimodal SCB distribution and lower molecular weight polymer, while the sites of $r_1r_2 = 1.0$ give the lower SCB concentration peak and higher molecular weight polymer.

Acknowledgment. We express our sincere appreciation to Prof. Shin Tsuge and Mr. Tadashi Takahashi for their very helpful comments. We also thank Mr. John Summers for assistance in preparing the manuscript and Mitsubishi Petrochemical Co. for permission to publish this work.

Registry No. (1-Butene)(ethylene) (copolymer), 25087-34-7; (1-hexene)(ethylene) (copolymer), 25213-02-9.

References and Notes

(1) Hsieh, E. T.; Randall, J. C. *Macromolecules* **1982**, *15*, 353.
(2) Hsieh, E. T.; Randall, J. C. *Macromolecules* **1982**, *15*, 1402.
(3) Kakugo, M.; Naito, Y.; Mizunuma, K.; Miyatake, T. *Macromolecules* **1982**, *15*, 1150.
(4) Wild, L.; Ryle, T. R.; Knobeloch, D. C.; Peat, I. R. *J. Polym. Sci., Polym. Phys. Ed.* **1982**, *20*, 441.
(5) Wild, L.; Ryle, T. R.; Knobeloch, D. C. *Polym. Prepr. (Am. Chem. Soc., Div. Polym. Chem.)* **1982**, *23*, 133.
(6) Nakano, S.; Goto, Y. *J. Appl. Polym. Sci.* **1981**, *26*, 4217.
(7) (a) Union Carbide Japanese Patent 54-148093, 1979. (b) Showa Denko Japanese Patent 55-3459, 1980. (c) CdF Chimie Japanese Patent 55-131007, 1980. (d) Mitsui Petrochemical Japanese Patent 53-92887, 1978.
(8) Usami, T.; Takayama, S. *Macromolecules* **1984**, *17*, 1756.
(9) Wilkes, C.; Carman, C.; Harrington, R. *J. Polym. Sci., Polym. Symp.* **1973**, *No. 43*, 237.

Crystal Lattice Modulus of Polyethylene Calculated As Functions of Crystallinity and Molecular Orientation by Linear Elastic Theory

Chie Sawatari and Masaru Matsuo*

Department of Clothing Science, Faculty of Home Economics, Nara Women's University, Nara 630, Japan. *Received May 6, 1986*

ABSTRACT: A mathematical representation based on a linear elastic theory is proposed by which one may investigate the dependence of the crystal lattice modulus in the chain direction on molecular orientation and crystallinity. This description indicates that the crystal lattice modulus as measured by X-ray diffraction is different from the intrinsic crystal lattice modulus. However, the numerical calculation indicates that the calculated value is almost independent of the molecular orientation and crystallinity except in the case of a low degree of molecular orientation and low crystallinity, although the calculated Young's modulus is strongly affected by them. Thus it turns out that X-ray diffraction has advantages in measuring the crystal lattice modulus exactly.

Introduction

The elastic moduli of a crystal lattice in the direction of the molecular chain axis have been reported from the theoretical and experimental viewpoints. Lyons,[1] Treloar,[2] Shimanouchi et al.,[3,4] and Miyazawa[5,6] have carried out theoretical treatments for various polymers using reliable force constants obtained mainly from infrared spectroscopy. Odajima et al.[7] calculated the elastic constants, C_{ij}, of polyethylene on the basis of Born's dynamical theory[8] for a model of interatomic interactions representing inter- and intramolecular force fields.

* To whom all correspondence should be addressed.

0024-9297/86/2219-2726$01.50/0

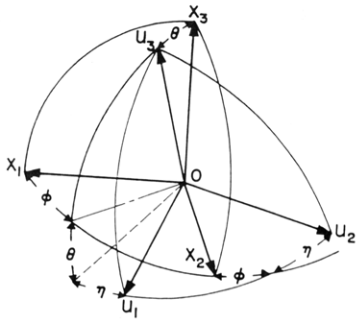

Figure 1. Eulerian angles θ, ϕ, and η specifying the orientation of Cartesian coordinate O–$u_1u_2u_3$, fixed in a structural unit, with respect to another coordinate O–$x_1x_2x_3$, fixed in the bulk specimen.

On the other hand, experimental results for crystal lattice moduli have been estimated for many polymers[9-12] on the basis of spectroscopic and mechanical methods. For example, Raman spectroscopy and inelastic neutron scattering are of the spectroscopic kind while X-ray diffraction may be regarded as mechanical. Estimation by X-ray diffraction has the advantage that the crystal lattice modulus can be measured directly from the stress–strain relationship. However, an essential question arises as to whether the homogeneous stress hypothesis is valid in such a case, that is, whether the stress within a specimen is everywhere the same as the external applied stress. In order to check this, ultradrawn polyethylene films with elongation ratios of 50, 100, 200, and 300 were used as specimens in previous work.[13] It turns out that the modulus is in the range 213–229 GPa and is independent of the degree of orientation of the crystal c axes, crystallinity, and crystal size as long as the draw ratio is greater than 50. These results indicated that a state of homogeneous stress can be assumed.

The present paper aims to demonstrate theoretically that the crystal lattice modulus is almost independent of draw ratio, molecular orientation, and crystallinity under external applied stress. A mathematical representation of the crystal lattice strain along the molecular chain axis is discussed in terms of the geometrical arrangement of the bulk specimen as revealed by X-ray analysis. Using the above system, we calculate the crystal lattice modulus and the Young's modulus as functions of draw ratio and crystallinity.

Crystal Modulus along the Molecular Chain Axis and the Young's Modulus in a Semicrystalline Polymer

A procedure for calculating the mechanical anisotropy of a two-phase system is derived on the basis of the homogeneous stress hypothesis by considering the structural units to be composed of crystalline and amorphous phases. Since the polymer molecules are intrinsically anisotropic in their mechanical properties, in each phase the bulk properties are anisotropic when the polymer molecules are not randomly oriented.

Figure 1 shows Cartesian coordinate O–$u_1u_2u_3$, fixed in a structural unit, with respect to another Cartesian coordinate O–$x_1x_2x_3$, fixed in the bulk specimen. The u_3 axis may be taken along the reference axis but has random orientation around the x_3 axis.

Let the composite structural unit be as shown in Figure 2, in which anisotropic noncrystalline layers lie adjacent to oriented crystalline layers with the interface perpendicular to the x_3 axis, so that the strains of the two phases at the boundary are identical. Considering the average mechanical properties of oriented crystalline and amorphous layers, one can replace Figure 2 by the simpler

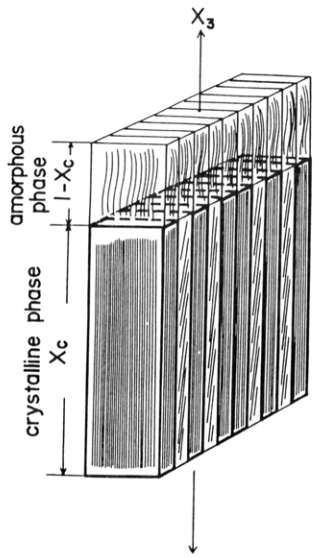

Figure 2. Schematic diagram of a proposed series model with multi-ply layers for anisotropy of a semicrystalline polymer.

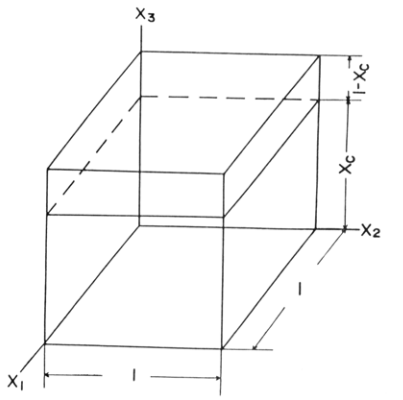

Figure 3. Composite structural unit of a semicrystalline polymer in which the crystalline and amorphous phases are connected at the face perpendicular to the x_3 axis.

model shown in Figure 3. In this model system, the mechanical constants of the two phases can be written by using the average mechanical constants of the crystal and amorphous phases. Accordingly, this model is convenient for considering the stress–strain relationships in both phases. The volume fraction X_c of crystallinity is represented by the fractional length X_c of the crystallites along the x_3 axis.

When the tensile stress σ_{33} is applied along the x_3 axis, the inner stresses of the crystalline and amorphous phases, (σ_{11}^c, σ_{22}^c, σ_{33}^c, 0, 0, 0) and (σ_{11}^a, σ_{22}^a, σ_{33}^a, 0, 0, 0), are applied to the two phases, respectively, to induce the following strains in each phase:

$$\epsilon_{11}^c = S_{11}^{cv}\sigma_{11}^c + S_{12}^{cv}\sigma_{22}^c + S_{13}^{cv}\sigma_{33}^c$$

$$\epsilon_{22}^c = S_{12}^{cv}\sigma_{11}^c + S_{11}^{cv}\sigma_{22}^c + S_{13}^{cv}\sigma_{33}^c$$

$$\epsilon_{33}^c = S_{13}^{cv}\sigma_{11}^c + S_{13}^{cv}\sigma_{22}^c + S_{33}^{cv}\sigma_{33}^c$$

$$\epsilon_{12}^c = \epsilon_{23}^c = \epsilon_{31}^c = 0 \qquad (1)$$

and

$$\epsilon_{11}^a = S_{11}^{av}\sigma_{11}^a + S_{12}^{av}\sigma_{22}^a + S_{13}^{av}\sigma_{33}^a$$

$$\epsilon_{22}^a = S_{12}^{av}\sigma_{11}^a + S_{11}^{av}\sigma_{22}^a + S_{13}^{av}\sigma_{33}^a$$

$$\epsilon_{33}^a = S_{13}^{av}\sigma_{11}^a + S_{13}^{av}\sigma_{22}^a + S_{33}^{av}\sigma_{33}^a$$

$$\epsilon_{12}^a = \epsilon_{23}^a = \epsilon_{31}^a = 0 \qquad (2)$$

where superscripts c and a represent the crystalline and amorphous phase, respectively. S_{uv}^{cv} and S_{uv}^{av} represent the average elastic compliances of the crystalline and amorphous phases, respectively. The uniaxial stress condition with respect to the x_3 axis leads to the following relations:

$$\sigma_{11} = X_c\sigma_{11}^{c} + (1 - X_c)\sigma_{11}^{a} = 0$$
$$\sigma_{22} = X_c\sigma_{22}^{c} + (1 - X_c)\sigma_{22}^{a} = 0$$
$$\sigma_{33} = \sigma_{33}^{c} = \sigma_{33}^{a} \quad (3)$$

where σ_{uv} corresponds to the stress of the bulk specimen. For the above restriction upon the strains, one has

$$\epsilon_{11} = \epsilon_{11}^{c} = \epsilon_{11}^{a}$$
$$\epsilon_{22} = \epsilon_{22}^{c} = \epsilon_{22}^{a}$$
$$\epsilon_{33} = X_c\epsilon_{33}^{c} + (1 - X_c)\epsilon_{33}^{a}$$
$$\epsilon_{12} = \epsilon_{23} = \epsilon_{31} = 0 \quad (4)$$

where ϵ_{uv} corresponds to the strain of the bulk specimen.

Assuming the homogeneous stress hypothesis for a polycrystalline material, the relation between the intrinsic compliance of a structural unit and the bulk compliance is given by

$$S_{ijkl}^{cv} = \sum_{r=1}^{3}\sum_{q=1}^{3}\sum_{p=1}^{3}\sum_{o=1}^{3}\langle a_{io}a_{jp}a_{kq}a_{lr}\rangle S_{opqr}^{co} \quad (5)$$

and

$$S_{ijkl}^{av} = \sum_{r=1}^{3}\sum_{q=1}^{3}\sum_{p=1}^{3}\sum_{o=1}^{3}\langle a_{io}a_{jp}a_{kq}a_{lr}\rangle S_{opqr}^{ao} \quad (6)$$

where S_{ijkl}^{cv} and S_{ijkl}^{av} are bulk compliances of the crystal and amorphous phases, respectively, and S_{opqr}^{co} and S_{opqr}^{ao} are their intrinsic compliances. a_{io} is, for example, the direction cosine of the u_o axis with respect to the x_i axis, which is given from the geometrical arrangements in Figure 1 as follows:

$$|a| = \begin{vmatrix} \cos\phi\cos\theta\cos\eta - \sin\phi\sin\eta & -\cos\phi\cos\theta\sin\eta - \sin\phi\sin\eta & \cos\phi\cos\theta \\ \sin\phi\cos\theta\cos\eta + \cos\phi\cos\eta & -\sin\phi\cos\theta\sin\eta + \cos\phi\cos\eta & \sin\phi\sin\theta \\ -\sin\theta\cos\eta & \sin\theta\sin\eta & \cos\theta \end{vmatrix} \quad (7)$$

Average values in eq 5 and 6, $\langle a_{io}a_{jp}a_{kq}a_{lr}\rangle$, can be given by

$$\langle a_{io}a_{jp}a_{kq}a_{lr}\rangle = \int_0^{2\pi}\int_0^{2\pi}\int_0^{\pi}\omega(\theta,\phi,\eta)a_{io}a_{jp}a_{kq}a_{lr}\sin\theta\,d\theta\,d\phi\,d\eta \quad (8)$$

where $\omega(\theta,\phi,\eta)$ is an orientation distribution function of the structural unit O–$u_1u_2u_3$ with respect to the coordinate O–$x_1x_2x_3$ in Figure 1.

In accordance with the analysis of Krigbaum and Roe,[14] the distribution function $\omega(\theta,\phi,\eta)$ may be expanded in a series of spherical harmonics. Introducing some changes from their notation, we can write the orientation factor using $\omega(\theta,\phi,\eta)$ in the case when the structural unit has a uniaxial orientation distribution around the x_3 axis:

$$F_{l0n} = \int_0^{2\pi}\int_0^{2\pi}\int_0^{\pi}\omega(\theta,\phi,\eta)P_l^n(\cos\theta)\cos(n\eta)\sin\theta\,d\theta\,d\phi\,d\eta \quad (l, n \text{ even}) \quad (9)$$

$P_l^n(\cos\theta)$ are the associated Legendre polynomials.

The elastic compliance S_{ijkl} represented as a tensor may be related to S_{uv} as follows:

$$S_{ijkl} = S_{uv} \quad u \text{ and } v \le 3$$
$$S_{ijkl} = (1/2)S_{uv} \quad u \text{ or } v \ge 3$$
$$S_{ijkl} = (1/4)S_{uv} \quad u \text{ and } v \ge 3 \quad (10)$$

where (ij) and (k_l) become u and v, respectively. The combinations are as follows:

$$(1\ 1) \rightarrow 1 \quad (2\ 2) \rightarrow 2 \quad (3\ 3) \rightarrow 3$$
$$(2\ 3) \rightarrow 4 \quad (3\ 1) \rightarrow 5 \quad (1\ 2) \rightarrow 6$$

Using eq 7–10, we can write eq 5 as follows:

$$S_{11}^{cv} = (1/64)S_{11}^{co}\{(1/35)F_{404} - (8/35)F_{402} + (72/35)F_{400} - (32/7)F_{202} + (64/7)F_{200} + 64/5\} + (1/64)S_{22}^{co}\{(1/35)F_{404} + (8/35)F_{402} + (72/35)F_{400} + (32/7)F_{202} + (64/7)F_{200} + 64/5\} + S_{33}^{co}\{(3/35)F_{400} - (2/7)F_{200} + 1/5\} + (1/64)(2S_{12}^{co} + S_{66}^{co})\{-(1/35)F_{404} + (24/35)F_{400} + (64/21)F_{200} + 64/15\} + (1/16)(2S_{13}^{co} + S_{55}^{co})\{(2/35)F_{402} - (24/35)F_{400} - (4/21)F_{202} - (8/21)F_{200} + 112/105\} + (1/16)(2S_{23}^{co} + S_{44}^{co})\{-(2/35)F_{402} - (24/35)F_{400} + (4/21)F_{202} - (8/21)F_{200} + 112/105\} \quad (11)$$

$$S_{33}^{cv} = (1/8)S_{11}^{co}\{(1/105)F_{404} - (8/105)F_{402} + (24/35)F_{400} + (8/7)F_{202} - (16/7)F_{200} + 56/35\} + (1/8)S_{22}^{co}\{(1/105)F_{404} + (8/105)F_{402} + (24/35)F_{400} - (8/7)F_{202} - (16/7)F_{200} + 56/35\} + S_{33}^{co}\{(8/35)F_{400} + (4/7)F_{200} + 1/5\} + (1/8)(2S_{12}^{co} + S_{66}^{co})\{-(1/105)F_{404} + (8/35)F_{400} - (16/21)F_{200} + 56/105\} + (1/2)(2S_{13}^{co} + S_{55}^{co})\{(2/105)F_{402} - (8/35)F_{400} + (1/21)F_{202} + (2/21)F_{200} + 2/15\} + (1/2)(2S_{23}^{co} + S_{44}^{co})\{-(2/105)F_{402} - (8/35)F_{400} - (1/21)F_{202} + (2/21)F_{200} + 2/15\} \quad (12)$$

$$S_{12}^{cv} = (1/64)S_{11}^{co}\{(1/105)F_{404} - (8/105)F_{402} + (24/35)F_{400} - (32/21)F_{202} + (64/21)F_{200} + 64/15\} + (1/64)S_{22}^{co}\{(1/105)F_{404} + (8/105)F_{402} + (24/35)F_{400} + (32/21)F_{202} + (64/21)F_{200} + 64/15\} + S_{33}^{co}\{(1/35)F_{400} - (2/21)F_{200} + 1/15\} + S_{12}^{co}\{-(1/3360)F_{404} + (1/140)F_{400} + (10/21)F_{200} + 4/15\} + S_{13}^{co}\{(1/420)F_{402} - (1/35)F_{400} - (5/42)F_{202} - (5/21)F_{200} + 4/15\} + S_{23}^{co}\{-(1/420)F_{402} - (1/35)F_{400} + (5/42)F_{202} - (5/21)F_{200} + 4/15\} \quad (13)$$

$$S_{13}^{cv} = S_{11}^{co}\{-(1/1680)F_{404} + (1/210)F_{402} - (3/70)F_{400} + (1/84)F_{202} - (1/42)F_{200} + 1/15\} + S_{22}^{co}\{-(1/1680)F_{404} - (1/210)F_{402} - (3/70)F_{400} - (1/84)F_{202} - (1/42)F_{200} + 1/15\} + S_{33}^{co}\{-(4/35)F_{400} + (1/21)F_{200} + 1/15\} + S_{12}^{co}\{(1/840)F_{404} - (1/35)F_{400} - (5/21)F_{200} + 4/15\} + S_{13}^{co}\{-(1/105)F_{402} + (4/35)F_{400} + (5/84)F_{202} + (5/42)F_{200} + 4/15\} + S_{23}^{co}\{(1/105)F_{402} + (4/35)F_{400} - (5/84)F_{202} + (5/42)F_{200} + 4/15\} \quad (14)$$

On the other hand, the amorphous-chain segments have uniaxial symmetry around the u_3 axis; thus eq 6 can be written as follows:

$$S_{11}^{av} = (1/8)(S_{11}^{ao} + S_{22}^{ao})\{(9/35)F_{400}^{am} + (8/7)F_{200}^{am} + 8/5\} + S_{33}^{ao}\{(3/35)F_{400}^{am} - (2/7)F_{200}^{am} + 1/5\} + (1/8)(2S_{12}^{ao} + S_{66}^{ao})\{(3/35)F_{400}^{am} + (8/21)F_{200}^{am} + 8/15\} + (1/2)(2S_{13}^{ao} + 2S_{23}^{ao} + S_{55}^{ao} + S_{66}^{ao})\{-(3/35)F_{400}^{am} - (1/21)F_{200}^{am} + 2/15\} \quad (15)$$

$$S_{33}^{av} = (S_{11}^{ao} + S_{22}^{ao})\{(3/35)F_{400}^{am} - (2/7)F_{200}^{am} + 1/5\} + S_{33}^{ao}\{(8/35)F_{400}^{am} + (4/7)F_{200}^{am} + 1/5\} + (2S_{12}^{ao} + S_{66}^{ao})\{(1/35)F_{400}^{am} - (2/21)F_{200}^{am} + 1/15\} + (2S_{13}^{ao} + 2S_{23}^{ao} + S_{44}^{ao} + S_{55}^{ao})\{-(4/35)F_{400}^{am} + (1/21)F_{200}^{am} + 1/15\} \quad (16)$$

$$S_{12}^{av} = (1/8)(S_{11}^{ao} + S_{22}^{ao})\{(3/35)F_{400}^{am} + (8/21)F_{200}^{am} + 8/15\} + S_{33}^{ao}\{(1/35)F_{400}^{am} - (2/21)F_{200}^{am} + 1/15\} + S_{12}^{ao}\{(1/140)F_{400}^{am} + (10/21)F_{200}^{am} + 4/15\} - (S_{13}^{ao} + S_{23}^{ao})\{(1/35)F_{400}^{am} + (5/21)F_{200}^{am} - 4/15\} \quad (17)$$

$$S_{13}^{av} = (S_{11}^{ao} + S_{22}^{ao})\{-(3/70)F_{400}^{am} - (1/42)F_{200}^{am} + 1/15\} + S_{33}^{ao}\{-(4/35)F_{400}^{am} + (1/21)F_{200}^{am} + 1/15\} - S_{12}^{ao}\{(1/35)F_{400}^{am} + (5/21)F_{200}^{am} - 4/15\} + (S_{13}^{ao} + S_{23}^{ao})\{(4/35)F_{400}^{am} + (5/42)F_{200}^{am} + 4/15\} \quad (18)$$

On the basis of eq 9, the orientation factors in eq 11–18 may be given as follows:

$$F_{200}\ (=F_{200}^{am}) = (1/2)(3\langle\cos^2\theta\rangle - 1) \quad (19)$$

$$F_{202}\ (=F_{202}^{am}) = 3\langle\sin^2\theta\cos 2\eta\rangle \quad (20)$$

$$F_{400}\ (=F_{400}^{am}) = (1/8)\{35\langle\cos^4\theta\rangle - 30\langle\cos^2\theta\rangle + 3\} \quad (21)$$

$$F_{402}\ (=F_{402}^{am}) = (15/2)\langle(7\cos^2\theta - 1)\sin^2\theta\cos 2\eta\rangle \quad (22)$$

$$F_{404}\ (=F_{404}^{am}) = 105\langle\sin^4\theta\cos 4\eta\rangle \quad (23)$$

Here, the problem is how the value of the intrinsic compliances S_{uv}^{co} and S_{uv}^{ao} of polyethylene can be determined theoretically. Unfortunately, there has been no report that the value of $1/S_{33}^{co}$ obtained by theoretical calculation is close to our experimental value in the range 213–229 GPa. Hence, the theoretical values of S_{uv}^{co} were estimated from the inverse matrix of the elastic stiffness C_{uv}^{co} proposed by Odajima et al.,[7] since their calculated value of $1/S_{33}^{co}$ provides the best fit to our experimental results among several theoretical results.[1-7]

According to their paper,[7] S_{uv}^{co} can be obtained as follows:

$$|S_{uv}^{co}| = \begin{vmatrix} S_{11}^{co} & S_{12}^{co} & S_{13}^{co} & 0 & 0 & 0 \\ S_{12}^{co} & S_{22}^{co} & S_{23}^{co} & 0 & 0 & 0 \\ S_{13}^{co} & S_{23}^{co} & S_{33}^{co} & 0 & 0 & 0 \\ 0 & 0 & 0 & S_{44}^{co} & 0 & 0 \\ 0 & 0 & 0 & 0 & S_{55}^{co} & 0 \\ 0 & 0 & 0 & 0 & 0 & S_{66}^{co} \end{vmatrix} =$$

$$\begin{vmatrix} 21.4 & -2.76 & -0.150 & 0 & 0 & 0 \\ -2.76 & 12.0 & -0.246 & 0 & 0 & 0 \\ -0.150 & -0.246 & 0.396 & 0 & 0 & 0 \\ 0 & 0 & 0 & 3.53 & 0 & 0 \\ 0 & 0 & 0 & 0 & 128.2 & 0 \\ 0 & 0 & 0 & 0 & 0 & 48.5 \end{vmatrix} \times 10^{-2}/\text{GPa} \quad (24)$$

The elastic compliances S_{uv}^{ao} of the amorphous phase are not quite certain. However, as our approximation, we can assume that the following relation between the potential energy $P(r)$ and the atomic or molecular distance r holds for a noncrystalline chain, although this treatment is a very crude approximation based on the hypothesis of a biphasic structure of crystalline and noncrystalline phases.[15]

$$P(r) = -c/r^n + d/r^m \quad (25)$$

where $m = 9$–12 and $n = 1$ or 6 for an ionic or molecular crystal, respectively. The elastic compliances S_{22}^{ao} and S_{11}^{ao} may be estimated by double differentiation of eq 25. Then

$$S_{11}^{ao} = S_{22}^{ao} = (\rho_c/\rho_a)^4 S_{11}^{c'} \quad (26)$$

In this treatment, the expansion of the amorphous phase is assumed to occur only along the lateral direction of the polymer chain, not lengthwise. The compliance S_{33}^{ao} may be estimated on the assumption that the modulus along the chain axes is proportional to the number of molecular chains on the unit area perpendicular to the chain axes. Then we have

$$S_{33}^{ao} = (\rho_c/\rho_a)S_{33}^{c'} \quad (27)$$

According to an estimation method by Hibi et al.,[16] the other compliances can be estimated as

$$S_{12}^{ao} = -\nu_{21}^{ao}S_{11}^{ao} \quad (28)$$

$$S_{23}^{ao} = S_{13}^{ao} = -\nu_{31}^{ao}S_{33}^{ao} \quad (29)$$

$$S_{55}^{ao} = S_{44}^{ao} = 2(S_{11}^{ao} + \nu_{31}^{ao}S_{33}^{ao}) \quad (30)$$

and

$$S_{66}^{ao} = 2S_{11}^{ao}(1 + \nu_{21}^{ao}) \quad (31)$$

The Poisson ratios ν_{21}^{ao} and ν_{31}^{ao} are set to be 0.45 on the assumption that the mechanical property of the amorphous phase is similar to an ideal rubber elasticity but a little bit tougher. The compliances $S_{uv}^{c'}$ in eq 26–31 correspond to S_{uv}^{cv} at $\theta = 0°$. Thus

$$S_{11}^{c'} = (1/8)(3S_{11}^{co} + 3S_{22}^{co} + 2S_{12}^{co} + S_{66}^{co})$$

$$S_{33}^{c'} = S_{33}^{co}$$

$$S_{12}^{c'} = (1/2)(S_{13}^{co} + S_{23}^{co})$$

$$S_{44}^{c'} = (1/2)(S_{44}^{co} + S_{55}^{co})$$

$$S_{66}^{c'} = (1/8)(2S_{11}^{co} + 2S_{22}^{co} + 3S_{66}^{co}) \quad (32)$$

Through the series of procedures discussed above, all parameters can be known, and then the elastic compliance S_{33} in the bulk specimen may be calculated by eq 1–4 as follows:

$$S_{33} = (\epsilon_{33}/\sigma_{33}) = X_c\{H(S_{uv}^{cv}, S_{uv}^{av}, X_c) + S_{33}^{cv}\} + (1 - X_c)\{G(S_{uv}^{cv}, S_{uv}^{av}, X_c) + S_{33}^{av}\} \quad (33)$$

where

$$H(S_{uv}^{cv}, S_{uv}^{av}, X_c) = 2S_{13}^{cv}(S_{13}^{av} - S_{13}^{cv})/\left\{S_{12}^{cv} + S_{11}^{cv} + \frac{X_c}{1 - X_c}(S_{11}^{av} + S_{12}^{av})\right\} \quad (34)$$

and

$$G(S_{uv}^{cv}, S_{uv}^{av}, X_c) = \frac{2X_c}{1 - X_c}S_{13}^{av}(S_{13}^{cv} - S_{13}^{av})/\left\{S_{12}^{cv} + S_{11}^{cv} + \frac{X_c}{1 - X_c}(S_{11}^{av} + S_{12}^{av})\right\} \quad (35)$$

Then the Young's modulus E is given by

$$E = 1/S_{33} \quad (36)$$

Returning to Figure 2, we note that the crystal (002) plane can be detected by X-ray diffraction only in the case

Table I
Characterization of Specimens Used To Measure the Crystal Lattice Modulus in the Previous Paper[13]

specimen	elongation ratio	crystal lattice modulus, GPa	volume crystallinity	orientation factor F_{200}	Young's modulus, GPa
A-1	50	222	88.9	0.99435	
A-2	50	205	84.9	0.99569	25–30
B-1	100	201	93.4	0.99980	
B-2	100	225	88.4	0.99747	45–55
C-1	200	213	91.1	0.99862	
C-2	200	213	94.1	0.99899	110–120
C-3	200	219	91.1	0.99985	
C-4	200	222	94.1	0.99957	
C-5	200	214	91.1	0.99792	
C-6	200	217	94.1	0.99756	
D-1	300	200	94.7	0.99999	
D-2	300	215	94.7	0.99963	151–202
D-3	300	229	95.6	0.99942	
E-1	400		97.2	0.99999	216

where the crystal chain axes are oriented perfectly in the stretching direction. Accordingly, in the stress field σ_{uv}^{c} of the crystal phase, the crystal lattice strain ϵ_{33}^{co} of the crystal (002) plane, which can be detected by X-ray measurement, can be represented as follows:

$$\epsilon_{33}^{co} = S_{13}^{co}\sigma_{11}^{c} + S_{23}^{co}\sigma_{22}^{c} + S_{33}^{co}\sigma_{33}^{c} \quad (37)$$

In eq 37, σ_{11}^{c} and σ_{22}^{c} can be represented as a function of σ_{33}^{c} by using eq 1–4; then we have

$$S_{33}^{c} = \epsilon_{33}^{co}/\sigma_{33}^{c} = -F(S_{uv}^{co},S_{uv}^{cv},S_{uv}^{av},X_c) + S_{33}^{co} \quad (38)$$

$$1/E_c = -F(S_{uv}^{co},S_{uv}^{cv},S_{uv}^{av},X_c) + 1/E_{co} \quad (39)$$

where

$$F(S_{uv}^{co},S_{uv}^{cv},S_{uv}^{av},X_c) = (S_{13}^{co} + S_{23}^{co}) \times (S_{13}^{cv} - S_{13}^{av})/\left\{S_{11}^{cv} + S_{12}^{cv} + \frac{X_c}{1 - X_c}(S_{11}^{av} + S_{12}^{av})\right\} \quad (40)$$

Here we note that the crystal lattice modulus of the crystal (002) plane detected by X-ray diffraction is essentially not equal to the intrinsic crystal lattice modulus E_{co}. Only in the case of $F(S_{uv}^{co},S_{uv}^{cv},S_{cv}^{av},X_c) \ll S_{33}$ (or $1/E_{co}$) is the measurable lattice modulus almost equal to the intrinsic crystal lattice modulus. Accordingly, we shall check whether this relation can be constructed through the numerical calculation.

Results and Discussion

Table I lists the experimental results about the crystal lattice modulus, the Young's modulus, volume crystallinity, and the second-order orientation factor of the crystal c axes in the previous work.[13] In addition to the above information, the orientation factor of amorphous chain segments must be given to calculate the crystal lattice modulus theoretically in our model system. The evaluation of the orientation of amorphous chain segments was obtained from the birefringence as estimated by subtraction of the crystalline contribution from the total birefringence, assuming simple additivity as indicated in the following equation:[17]

$$\Delta_{total} = X_c\Delta_c + (1 - X_c)\Delta_a + \Delta_f \quad (41)$$

where Δ_{total} is the total birefringence of the bulk specimen, Δ_c is the crystalline birefringence, Δ_a is the amorphous birefringence, and Δ_f is the form birefringence. In eq 41, Δ_c and Δ_a can be given by

$$\Delta_c = \Delta_c^{\circ}F_{200} \quad (42)$$

and

$$\Delta_a = \Delta_a^{\circ}F_{200}^{am} \quad (43)$$

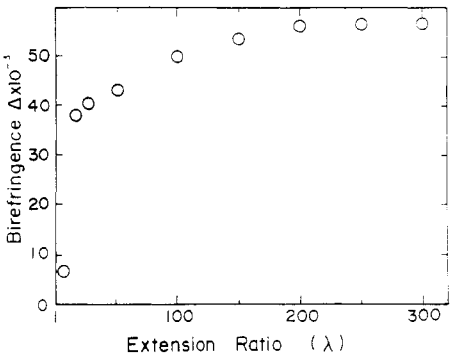

Figure 4. Birefringence of drawn polyethylene gel films as a function of draw ratio λ.

where Δ_c° and Δ_a° are the intrinsic birefringence of the crystal and amorphous phases, respectively, in the x_3 axis.

Figure 4 shows the change in the total birefringence Δ_{total} with increasing draw ratio λ. The values for specimens drawn beyond λ = 200 are close to 58.5×10^{-3}, which corresponds to the intrinsic crystal birefringence Δ_c° calculated from the three principal refractive indices of crystals of the n-paraffin $C_{36}H_{74}$ reported by Bunn and de Daubeny.[18] According to these authors the refractive indices n_a, n_b, and n_c are 1.514, 1.519, and 1.575, respectively. The birefringence, given by $n_c - (n_a + n_b)/2$, is thus equal to 58.5×10^{-3}. The defect of such a treatment is that the principal refractive indices were estimated only by assuming the atomic arrangements within the crystal unit and neglecting the uncertain effects of the internal field. Furthermore, the form birefringence cannot be neglected, as a number of voids within the drawn specimens have been observed by scanning electron microscopy.[19] Unfortunately, there is no way to estimate the form birefringence in our laboratory, since we have not been able to measure it exactly. In the case when Δ_c° and Δ_f cannot be obtained exactly, a reasonable second-order orientation factor F_{200}^{am} likewise cannot be estimated. Accordingly, we are obliged to propose a crude approximation as a model that both the orientation factors F_{200} and F_{200}^{am} show the same behavior defined by an affine mode:

$$\omega(\cos\theta) = \frac{\lambda^3}{\{\lambda^3 - (\lambda^3 - 1)\cos^2\theta\}^{3/2}} \quad (44)$$

where λ is a draw ratio.

Table II lists the calculated results of the orientation factor F_{200} (and F_{200}^{am}) against λ. Comparing Table I with Table II, it is evident that the experimental values of F_{200} for all draw ratios are higher than the calculated ones, but the difference is very small. Accordingly, all factors in eq

Table II
Second-Order Orientation Factor Calculated on the Basis of Eq 44

draw ratio λ	orientation factor F_{200} (and F_{200}^{am})	draw ratio λ	orientation factor F_{200} (and F_{200}^{am})
2	0.43065	100	0.99765
5	0.81096	200	0.99917
10	0.92838	300	0.99955
20	0.97403	400	0.99970
50	0.99336		

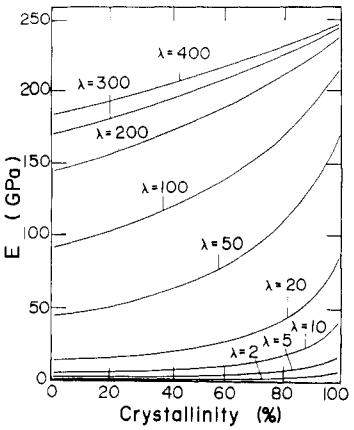

Figure 5. Young's modulus E calculated as a function of crystallinity for various draw ratios λ.

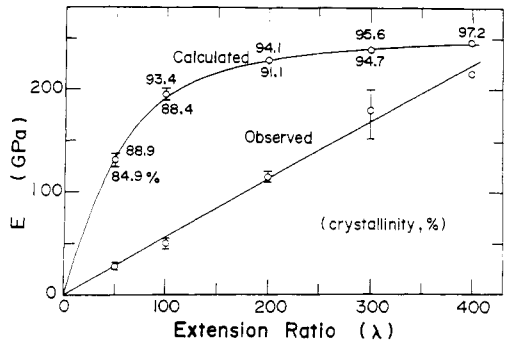

Figure 6. Young's modulus E observed and calculated as a function of draw ratio λ.

11–14 are obtained from eq 44.

Figure 5 shows crystallinity dependence of the Young's modulus E against various values of λ. The Young's modulus E increases as the crystallinity increases. This tendency becomes considerable with increasing λ. In the range from λ = 50 to λ = 100, the magnitude of the increase becomes very high but the crystallinity dependence of the Young's modulus becomes less pronounced with further increases of λ beyond 200. In the case of λ = 400, E is close to the theoretical value proposed by Odajima et al.[7] as the crystallinity increases.

Figure 6 shows the change in the Young's modulus with increasing λ. The indispensable crystallinities to calculate E for each λ from eq 36 are selected from the experimental values in Table I. The value of E is hardly affected by the small uncertainty in the values of crystallinity. The number shows the value of crystallinity which was used in the calculation. The calculated value increases considerably up to λ = 100 and it tends to level off with further increases of λ. In contrast, the observed value shows a linear increase. This disagreement is due to two factors. One is the crude approximation of the orientation of the amorphous chain segments. The other is that eq 5 and 6, indicating the dependence of the mechanical constant on the fourth- and second-order tensors, are not

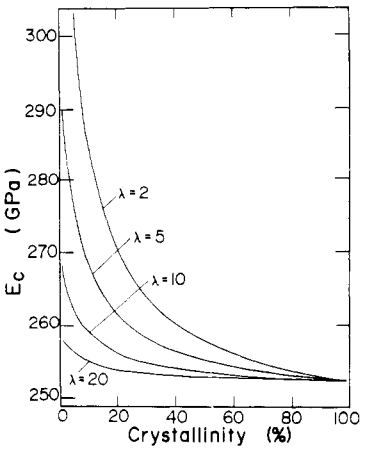

Figure 7. Crystal lattice modulus E_c calculated as a function of crystallinity for various draw ratios up to 20.

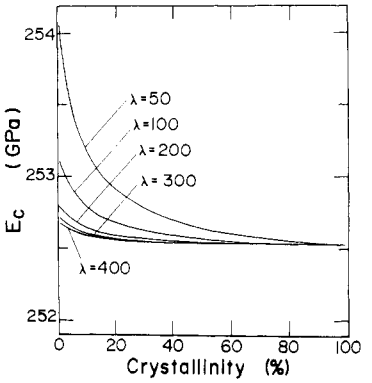

Figure 8. Crystal lattice modulus E_c calculated as a function of crystallinity for various draw ratios between 50 and 400.

enough to estimate the mechanical property of the bulk specimen exactly. It may be expected that the Young's modulus is dependent upon a number of factors such as crystal defects, crystal disorder, and chain scission in addition to the orientation of molecular chains.

Figures 7 and 8 show the crystallinity dependence of the crystal lattice modulus E_c for various draw ratios. The value of E_c increases with decreasing crystallinity but this tendency is not so significant. Especially, as shown in Figure 7, E_c for specimens drawn beyond λ = 20 is hardly affected by the crystallinity. That is, such a small difference is perfectly within experimental error.

Returning to eq 39, we can understand that the crystal lattice modulus E_c measured by X-ray diffraction is not equal to the intrinsic crystal lattice modulus $E_c°$ evaluated theoretically. However, if $F(S_{uv}^{co},S_{uv}^{cv},S_{uv}^{av},X_c) \ll 1/E_c°$, E_c is almost equal to $E_c°$. Figure 9 shows the change in log F against crystallinity for various draw ratios to make clear the relationship between $1/E_c°$ (or S_{33}^{co}) and F. With increasing λ and crystallinity, the value of F is much lower than that of S_{33}^{co} (=0.396 × 10^{-2}/GPa). Hence, the crystal lattice modulus E_c is close to a constant value, $1/E_c°$, with increasing λ and crystallinity. This numerical result is important to understand that the measurable crystal lattice modulus of polyethylene is independent of draw ratio and crystallinity and is almost equal to the intrinsic crystal lattice modulus in the chain axis direction, as long as the draw ratio of test specimens is beyond λ = 5. Because most drawn polyethylene samples have greater than 50% crystallinity, this result supports the advantage of measuring the crystal lattice modulus by X-ray diffraction.

In conclusion, on the basis of the numerical calculation by the linear elastic theory, it is found that the crystal

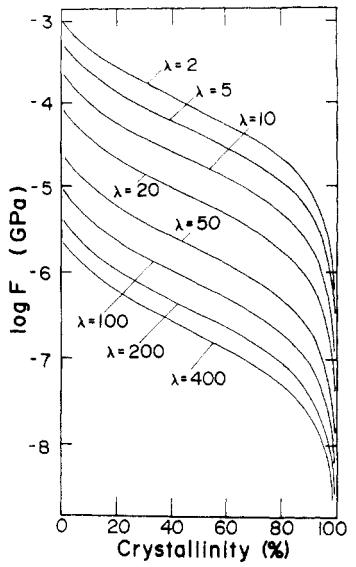

Figure 9. Logarithmic value of F calculated as a function of crystallinity for various draw ratios λ.

lattice modulus as measured by X-ray diffraction is independent of molecular orientation and crystallinity and that the Young's modulus approaches the crystal lattice modulus with increasing draw ratio at 100% crystallinity. These results support, on the whole, the experimental results measured for ultradrawn polyethylene films in previous work.[13] Furthermore, a slight discrepancy between the calculated and experimental results indicate that the Young's modulus is also sensitive to crystal defects, crystal disorder, and chain scission in addition to the molecular orientation and crystallinity. Accordingly, the simple relationship represented by eq 5 and 6 must be reconsidered in order to realize good agreement between the calculated and observed values. The effect of a number of parameters such as the defects, the disorder, and chain scission on mechanical properties are perhaps the most significant of the unknown contributions and must be taken into account in further studies.

Registry No. Polyethylene, 9002-88-4.

References and Notes

(1) Lyons, W. J. *J. Appl. Phys.* **1958**, *29*, 1429.
(2) Treloar, L. R. G. *Polymer* **1960**, *1*, 95.
(3) Shimanouchi, T.; Asahina, M.; Enomoto, S. *J. Polym. Sci.* **1962**, *59*, 93.
(4) Asahina, M.; Enomoto, S. *J. Polym. Sci.* **1962**, *59*, 101.
(5) Miyazawa, T., *Rep. Prog. Polym. Phys. Jpn.* **1965**, *8*, 47.
(6) Miyazawa, T. Paper presented at the 13th Symposium of the Society of Polymer Science, Japan, Tokyo, 1964, Proceedings, p 60.
(7) Odajima, S.; Maeda, T. *J. Polym. Sci., Part C* **1966**, *15*, 55.
(8) Born, M.; Huang, T. *Dynamic Theory of Crystal Lattices*; Clarendon: Oxford, 1956.
(9) Sakurada, I.; Nukushina, Y.; Ito, T. *J. Polym. Sci.* **1962**, *57*, 651.
(10) Sakurada, I.; Ito, T.; Nakamae, K. *J. Polym. Sci., Part C* **1966**, *15*, 75.
(11) Storobl, G. R.; Eckel, R. *J. Polym. Sci., Polym. Phys. Ed.* **1976**, *14*, 913.
(12) Holiday, L.; White, J. W. *Pure Appl. Chem.* **1971**, *26*, 545.
(13) Matsuo, M.; Sawatari, C. *Macromolecules* **1986**, *19*, 2036.
(14) Krigbaum, W. R.; Roe, R. J. *J. Chem. Phys.* **1964**, *41*, 737.
(15) Nomura, S.; Kawabata, S.; Kawai, H.; Yamaguchi, Y.; Fukushima, A.; Takahara, H. *J. Polym. Sci., Part A-2* **1969**, *7*, 325.
(16) Hibi, S.; Maeda, M.; Mizuno, M.; Nomura, S.; Kawai, H. *Sen-i Gakkaishi* **1973**, *29*, 137.
(17) Stein, R. S.; Norris, F. H. *J. Polym. Sci.* **1956**, *21*, 381.
(18) Bunn, C. W.; de Daubeny, R. *Trans. Faraday Soc.* **1954**, *50*, 1173.
(19) Matsuo, M.; Inoue, K.; Abumiya, N. *Sen-i Gakkaishi* **1984**, *40*, 275.

On Deformation of Polyethylene: The Question of Melting and Recrystallization

Hoe Hin Chuah,† J. S. Lin,‡ and Roger S. Porter*

Polymer Science and Engineering Department, University of Massachusetts, Amherst, Massachusetts 01003. *Received January 18, 1986*

ABSTRACT: The question of melting and recrystallization of polyethylene on drawing is evaluated by using samples with a range of starting morphologies. They were prepared by crystallization at an elevated pressure of 460 MPa and at different temperatures to produce chain-extended polyethylene with lamellar thicknesses ranging from 270 to 480 nm. Chain-folded polyethylene was also prepared by quenching its melt. These samples were examined after being uniaxially drawn by solid-state extrusion at constant temperatures from 70 to 125 °C. Weak meridional intensity maxima were found in small-angle X-ray scattering patterns of the chain-extended polyethylene after drawing, which originates from the deformation of a small fraction of low molecular weight polyethylene rejected during crystallization. From thermal analyses and consideration of X-ray scattering patterns of both the drawn chain-extended and chain-folded polyethylene, the chain-extended lamellae do not appear to undergo melting and recrystallization for the draw conditions used.

Introduction

Several deformation mechanisms have been proposed to describe the morphological changes during drawing of semicrystalline polymers. The most widely accepted one and most suited for polyethylene (PE) is the model of Peterlin.[1] It involves shearing, rotation, chain tilt, and slip in the lamellae and their transformation into bundles of microfibrils. For many years, it has been disputed whether such morphological changes on deformation involve melting and recrystallization.

Advances in drawing have produced PE with uniaxial draw ratio many times above its "natural draw". This feature was thought to be possible only if the local strain

† Now at the Research Institute, University of Dayton, Dayton, OH 45469.
‡ National Center for Small-Angle Scattering Research, Solid State Division, Oak Ridge National Laboratory, Oak Ridge, TN 37830.

0024-9297/86/2219-2732$01.50/0